Trans. JSASS Aerospace Tech. Japan
Vol. 14, No. ists30, pp. Pb_63-Pb_68, 2016

Optimization of Plasma Production with Impedance Analysis for a Micro RF Ion Thruster

By Kaito NAKAGAWA[1)] and Yoshinori TAKAO[2)]

[1)]*Department of Systems Integration, Yokohama National University, Yokohama, Japan*
[2)]*Division of Systems Research, Yokohama National University, Yokohama, Japan*

(Received July 31st, 2015)

We have investigated the plasma production in a micro RF ion thruster, where the plasma source is 5.0 mm in radius and 10 mm in length. To find the optimum condition to generate the RF plasma in the wide range of frequency f = 1-1000 MHz and pressure p = 0.1-10.0 Pa, we employ the equivalent circuit model, where the global model is also incorporated to obtain the plasma parameters self-consistently. The numerical results have indicated that capacitive coupling dominated over inductive coupling and the sheath resistance has a significant influence on the power coupling efficiency at lower frequency. The power coupling efficiency could be more than 80% at higher frequencies (> 30 MHz) .

Key Words: Ion Thruster, RF Plasma, Circuit Model, Global Model

Nomenclature

C	:	capacitance
e	:	elementary electric charge
f	:	frequency
I	:	current
j	:	imaginary number
L	:	inductance
M	:	mutual inductance
n	:	number density
P	:	power
R	:	resistance
T	:	temperature
V	:	voltage
X	:	reactance
Z	:	impedance
ω	:	angular frequency
Subscripts		
abs	:	plasma absorption
cap	:	capacitive
e	:	electron
g	:	neutral gas
i	:	ion
ind	:	inductive
sh1	:	sheath next to dielectric
sh2	:	sheath next to ground
$*$	:	excited state

1. Introduction

Recently miniature satellites (less than 100 kg) have been attracting a lot of interest from the space engineering community. These miniature satellites can be manufactured and operated by small organization, such as universities and small companies. However, because of the limit of weight, volume, and power, almost all of miniature satellites do not have any propulsion system. Therefore, the miniature satellites cannot change their orbit by themselves. That is why, the development of high-performance microthrusters is required.[1)] Since ion thrusters are one of the most promising microthrusters, we have developed a micro RF ion thruster (Fig. 1).[2)] This micro RF ion thruster has the radius and the length of its discharge chamber of 5 mm and 10 mm, respectively, which is one of the smallest RF ion thrusters in the world. Since the micro RF ion thruster does not have any magnets or electrodes, it has light structure and high reliability, which is one of the biggest advantages.

Owing to the strong limitations mentioned above, the efficiency of plasma generation the thruster efficiency has to be high. Whereas conventional RF ion thrusters have already been studied experimentally and numerically, there are few studies on a 1-cm class micro RF ion thruster.[3)] In view of the power supply limitation, it is important to increase the efficiency of plasma generation. Therefore, we have to investigate the best condition where the micro RF plasma is produced efficiently. RF ion thrusters with typical size of diameter (more than a few cm) have already been reserched numerically using a global model.[4,5)] These studies focus on the plasma generation only and do not include the RF circuits. On the other hand, in this study, we employ a hybrid model consisting of not only a global model (GM) but also an equivalent circuit model, where we can analyze the characteristics of the RF plasma generation self-consistently. This hybrid model, which also takes into account the matching circuit, enables us to obtain the total efficiency of the RF ion thruster system, where we can analyze both circuit and plasma losses. In this study, we have improved our numerical model by incorporating a global model (GM) into an equivalent circuit model, where we can analyze the characteristics of the RF plasma generation self-consistently. In the previous paper,[2)] the circuit model was employed based on the fixed plasma density and temperature, which were obtained from a particle-in-cell (PIC) simulation. Since the global model treats the plasma in a volume averaged manner as described later, the

Copyright© 2016 by the Japan Society for Aeronautical and Space Sciences and ISTS. All rights reserved.

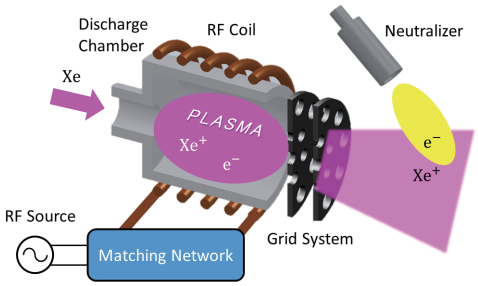

Fig. 1. Schematic of the micro RF ion thruster.

calculation time is several orders of magnitude shorter than the PIC simulation time. Thus, the circuit model with the global model would be appropriate to find the optimum condition of plasma production under a wide range of conditions.

2. Assumptions

To simplify the model, we assume the following conditions.

- The plasma is treated as a continuum.
- The plasma is macroscopically neutral, i.e. the electron density n_e equals the ion density n_i.
- The charged particles diffuse towards the walls according to the ambipolar diffusion theory.
- In the plasma source, the plasma parameters are treated in a volume-averaged or non-dimensional manner.
- Neutral particles have Maxwellian velocity distribution at the gas temperature of 300 K.
- The reactions between electrons and neutral particles taken into account are elastic scattering, excitation and ionization for electron.

$$\begin{aligned} e^- + Xe &\rightarrow e^- + Xe && \text{(Elastic Scattering)} \\ e^- + Xe &\rightarrow e^- + Xe^* && \text{(Excitation)} \\ e^- + Xe &\rightarrow e^- + Xe^+ + e^- && \text{(Ionization)} \end{aligned}$$

- The sheath is treated based on the Child-Langmuir model.
- Plasma is in an equilibrium state, and we do not consider transient states.

3. Equivalent Circuit Model

It is known that inductive discharges have two discharge modes, an H-mode and an E-mode. In the H-mode inductive coupling is dominant over capacitive coupling, leading to high density plasma (ICP), while in the E-mode capacitive coupling is dominant, producing low density plasma (CCP).[6] Figure 2 shows a schematic of the RF discharge model and its simplified equivalent circuit model.[7] We assume that an inductive current I_{ind} flows azimuthally along an RF coil whereas a capacitive current I_{cap} flows from the RF coil to a grounded metal through the quartz tube, sheaths and bulk plasma. Since the RF plasma discharge requires a matching network to transfer the RF power efficiently to the plasma from the source, a Γ-shaped matching network is employed.

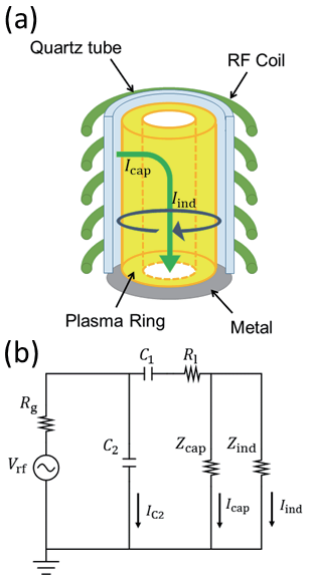

Fig. 2. (a) Schematic of the RF discharge model and (b) its simplified equivalent circuit model, including RF power source and matching circuit.

3.1. ICP circuit model

Figure 3 shows the circuit model of the inductive coupling, describing Z_{ind} shown in Fig. 2(b) The ICP circuit corresponds to a transformer which consists of the primary circuit of the N-turn RF coil with inductance L_{coil} and resistance R_{coil} and the secondary circuit of the one-turn plasma coil with inductance $L_1 + L_{e1}$ and resistance R_{p1}. L_1 is the geometrical inductance due to the plasma current path, and L_{e1} is the electron inertia inductance. The mutual induction between the primary and secondary coil is represented by the mutual inductance M. It is difficult to calculate the whole impedance of inductive coupling directly, but using equivalent transformed circuit, we can easily calculate the impedance Z_{ind} like as below

$$Z_{ind} = Z_p + R_{coil} + j\omega L_{coil}, \tag{1}$$

where Z_p is obtained from the following equation:

$$\frac{1}{Z_p} = \frac{1}{j\omega M} + \frac{1}{j\omega(L_1 - M + L_{e1}) + R_{p1}}. \tag{2}$$

The RF coil resistance R_{coil} and inductance L_{coil} can be described as below:

$$R_{coil} = \rho \frac{2\pi r_{coil} N}{S_{coil}} \tag{3}$$

$$L_{coil} = k_N \mu_0 \frac{\pi N^2 r_{coil}^2}{h_{coil}} \tag{4}$$

where ρ is the resistivity of the copper wire, r_{coil} is the radius of the RF coil, S_{coil} is the effective cross section area of the wire which is $2\pi r_{coil} d_{sk}$ with a skin depth d_{sk}, k_N is Nagaoka coefficient , μ_0 is the permeability in vacuum, h_{coil} is the height of the RF coil. The absorbed complex power in the ICP is defined as

$$P_{ind} = (Z_{ind}\, I_{ind}) \cdot \tilde{I}_{ind}, \tag{5}$$

where I_{ind} is the current through the primary coil, and $\tilde{I}_{ind}$ is the conjugate complex number of I_{ind}.

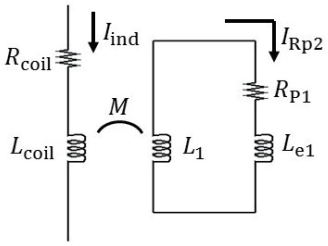

Fig. 3. The circuit model of the inductive coupling, describing Z_{ind} in Fig. 2(b).

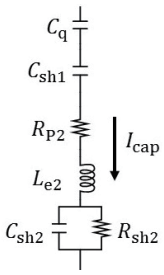

Fig. 4. The circuit model of the capacitive coupling, describing Z_{ind} in Fig. 2(b).

3.2. CCP circuit model

Figure 4 shows the circuit model of the capacitive coupling, describing Z_{cap} shown in Fig. 2(b), where it can be modeled as a series circuit. In this circuit, C_{q} is the quartz capacitance, C_{sh1} is the sheath capacitance next to the quartz, R_{p2} is the bulk plasma resistance due to ohmic heating, L_1 is the plasma inductance due to the electron inertia, C_{sh2} is the plasma-to-ground sheath capacitance and R_{sh2} is the sheath resistance due to the stochastic process (collisionless heating). Here, expressions for R_{p2} and L_{e2} are the same as those for R_{p1} and L_{e1}, but values for R_{p2} and L_{e2} are not equal to those for R_{p1} and L_1 in ICP because of the difference in the current path length and area between ICP and CCP. It should be noted that the plasma impedance, such as R_{p}, L_{e}, R_{sh} etc., is functions of electron density and temperature. The details of the expressions are described in.[7)]

3.3. Matching circuit

For RF circuits, maximizing deliverable power to a load is an important issue. We consider a simplified circuit having a load with the impedance $Z = R + jX$, voltage of the RF power source V, and the internal resistance of the source R_{g}. The power consumption of the load is then described as

$$P = \frac{V^2 R}{(R_{\mathrm{g}} + R)^2 + X^2}. \tag{6}$$

If $R = R_{\mathrm{g}}$ and $X = 0$, the power consumption is calculated to be $P = V^2/4R$ as the maximum value. Since we consider matching the load impedance $Z_{\mathrm{s}} = R_{\mathrm{s}} + jX_{\mathrm{s}}$ to the internal resistance R_{g} by the Γ-shaped matching circuit (Fig. 5). The variable capacitance C_1 and C_2 are determined to be

$$C_1 = \frac{1}{\omega\left(X_{\mathrm{s}} - \sqrt{R_{\mathrm{s}}R_{\mathrm{g}} - R_{\mathrm{s}}^2}\right)} \tag{7}$$

$$C_2 = \frac{\sqrt{R_{\mathrm{s}}R_{\mathrm{g}} - R_{\mathrm{s}}^2}}{\omega R_{\mathrm{s}}R_{\mathrm{g}}}. \tag{8}$$

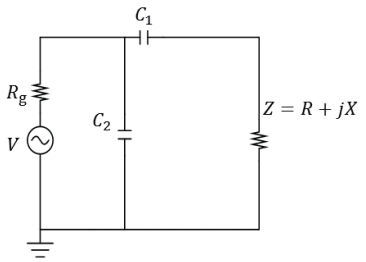

Fig. 5. The simplified model of matching circuit.

4. Global Model

The equivalent circuit model described above requires the electron density and temperature to decide the plasma impedance on one hand, while on the other hand these parameters are as a function of power absorbed in the plasma, which is dependent on the RF source power and the matching network. To specify the relation between the plasma parameter and the absorbed power, we employ the global model analysis, which is composed of the energy and particle balance equations.

4.1. Energy balance

When plasma remains in equilibrium state, the plasma absorbed power, P_{abs} equals the plasma dissipated power, P_{dis}. The plasma absorbed power can be calculated from the circuit model. On the other hand, the plasma dissipated power can be described below[8)]

$$P_{\mathrm{dis}} = e n_{\mathrm{e}} u_{\mathrm{B}} A_{\mathrm{eff}} \varepsilon_{\mathrm{tot}}, \tag{9}$$

where u_{B} is the Bohm velocity, A_{eff} is the effective area for the particle loss, $\varepsilon_{\mathrm{tot}}$ is the total energy loss per electron-ion pair from the system. Here, we assume that the energy loss is caused by the collision between electron and neutral particle, and the kinetic energy lost of electron and ion at a surface. From Eq. (9) and $P_{\mathrm{abs}} = P_{\mathrm{dis}}$, we obtain the plasma density as below:

$$n_{\mathrm{e}} = \frac{P_{\mathrm{abs}}}{e u_{\mathrm{B}} A_{\mathrm{eff}} \varepsilon_{\mathrm{tot}}}. \tag{10}$$

4.2. Particle balance

The time variation of the number of electron in the system can be described below[8)]

$$V_{\mathrm{chamber}} \frac{dn_{\mathrm{e}}}{dt} = K_{\mathrm{iz}} n_{\mathrm{e}} n_{\mathrm{g}} V_{\mathrm{chamber}} - n_{\mathrm{e}} u_{\mathrm{B}} A_{\mathrm{eff}} \tag{11}$$

where V_{chamber} is the volume of discharge chamber, K_{iz} is the rate constant of ionization, n_{g} is the number density of neutral gas. The first term of the right-hand side means a number of electron that is created in the system, and the second term means a number of electron that disappears in the system. In the equilibrium state, the left-hand side becomes zero. Hence, the relation of the particle balance can be express as:

$$\frac{K_{\mathrm{iz}}}{u_{\mathrm{B}}} = \frac{A_{\mathrm{eff}}}{n_{\mathrm{g}} V_{\mathrm{chamber}}}. \tag{12}$$

Since we assume that electrons have Maxwellian velocity distribution, we consider that K_{iz} is a function of the electron temperature as below:[8)]

$$K_{\mathrm{iz}} = 2.34^{-14} T_{\mathrm{e}}^{0.59} \exp\left(-\frac{\mathrm{E}_{\mathrm{iz}}}{T_{\mathrm{e}}}\right) \tag{13}$$

Table 1. The calculation conditions

Radius of the chamber (mm)	5.0
Length of the chamber (mm)	10
The number of coil winding	5
Thickness of dielectric (mm)	1.0
Propellant gas	Xe
The coupling coefficient[10]	0.2
The RF supplied power (mW)	200

where E_{iz} is the ionization energy of xenon and the constant values are fitted by using the ionization reaction rate data.[9] From Eqs.(12) and (13), we can obtain the self-consistent electron temperature based on the neutral gas density n_g, i.e., pressure.

5. Results and Discussion

Table 1 summarizes the calculation conditions. Since the power RF and the pressure of the neutral gas are variable, the analysis is carried out for the wide range of frequency f = 1-1000 MHz and pressure p = 0.1-10.0 Pa. Here, the coupling coefficient k_M is using to calculate the mutual inductance ($M = k_M \sqrt{L_{coil} L_1}$) between the RF coil and the one-turn plasma coil.

5.1. Effect of the global model

5.1.1. Electron density and temperature

Figures 6 and 7 show the electron density as a function of RF frequency and the electron temperature as a function of neutral gas pressure, respectively, where we also plot the fixed electron density of 3.0×10^{16} /m^3 and temperature of 3 eV as a reference obtained from the circuit model only. From these figures, we confirm that the electron density and temperature are dependent on the neutral gas pressure and/or RF frequency. The electron density significantly increases with increasing RF frequency, so that higher RF frequency is desirable for the plasma production. From Eq.(12), the electron temperature is a function of the neutral density or pressure only, and thus the electron temperature decreases monotonically with increasing the gas pressure owing to the increase in collisions with neutrals, being independent of the RF frequency.

It should be noted that the blank region around 100 MHz is due to the inability to match the load with the Γ-shaped matching circuit, where the resistance of the discharge plasma R_s is calculated to be more than 50 Ω, that is, C_1 and C_2 cannot be obtained as real numbers from Eqs.(7) and (8). If this matching circuit was converted to Π-shaped or T-shaped matching circuit, which can be matched to any load impedance,[11] this blank region would disappear.

5.1.2. Absorbed power and efficiency

Figures 8 and 9 show the inductive and capacitive absorbed power as a function of RF frequency, respectively, and power coupling efficiency is shown in Fig. 10.

Here, this efficiency is defined as $P_{abs}/P_{supplied}$,where $P_{supplied}$ is the power supplied to the discharge chamber, and this power is kept being equal to the half of the supplied power (200 mW) because we match the load to the internal resistance of 50 Ω in the calculations, where the load consist of the plasma resistance and the resistances of the coil and the other transmission lines. As shown these figures, the inductive absorbed power at lower

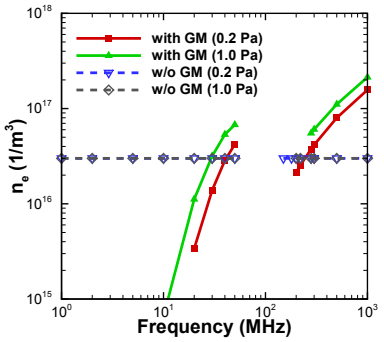

Fig. 6. The electron density vs. RF frequency.

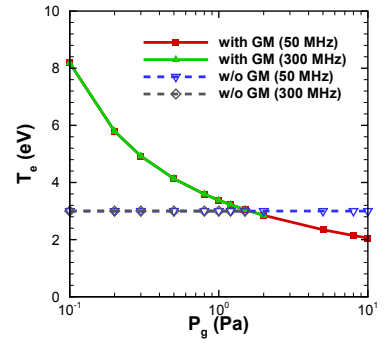

Fig. 7. The electron temperature vs. neutral gas pressure.

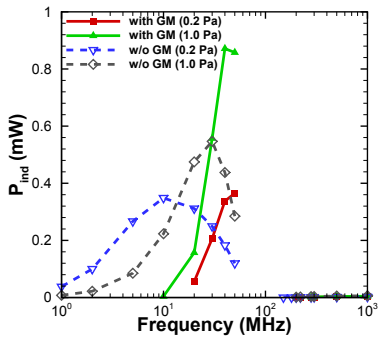

Fig. 8. The absorbed inductive power vs. RF frequency.

frequency is larger than at higher frequency. However, the value of the inductive absorbed power is less than 1 mW. Thus, the ratio of the capacitive absorbed power to the total absorbed power is more than 99% in all the frequency range examined. When frequency is more than 120 MHz, power coupling efficiency is more than 80%. On the other hand, when frequency is less than 30 MHz, efficiency is less than 20%. This low efficiency is due to the relatively large current, which leads to a large power loss to the resistances of the coil and the other transmission lines.[2] Thus, the difference in efficiency at below 30 MHz is hardly recognized in Fig. 10 even though the electron density obtained from the circuit model with the global model is much less than the fixed electron density of 3.0×10^{16} /m^3 at low frequency. Finally, the maximum power coupling efficiency was obtained at around 100 MHz, which is in agreement with the previous results.[2] Since the previous PIC simulation was validated by comparing the experimental results, the present model is also validated in terms of the dependence of power coupling efficiency on the RF frequency.[2]

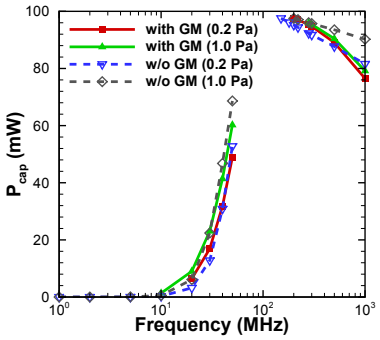

Fig. 9. The absorbed capacitive power vs. RF frequency.

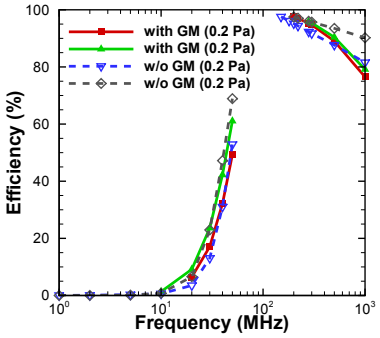

Fig. 10. The power coupling efficiency vs. RF frequency.

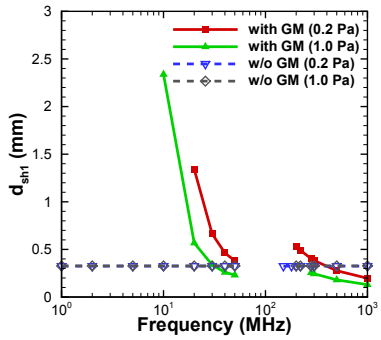

Fig. 11. The sheath thickness near to the dielectric.

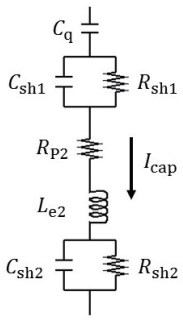

Fig. 12. The modified circuit model of CCP branch after adding the sheath resistance adjacent to the dielectric.

5.1.3. Sheath

Figure 11 shows the thickness of the sheath adjacent to the quartz tube as a function of RF frequency, where we also plot the sheath thickness obtained from the circuit model only with fixed electron density of 3.0×10^{16} /m^3 and temperature of 3 eV as a reference. The thickness significantly increases with decreasing RF frequency at below 50 MHz and it exceeds 2.0 mm because of the decrease in electron density and the increase in electron temperature as shown in Figs. 6 and 7, which results in longer Debye length. Note that the tendency is the same as the thickness of the sheath next to the grounded metal (not shown here). Since the radius and the half height of the discharge chamber are 5.0 mm, the ratio of the sheath to the chamber dimension is about 10% even at higher frequency. In other words, the ratio of the sheath to the plasma length in this very small size chamber is much larger than in typical size chamber. Therefore, as previously stated, capacitive coupling dominates over the inductive coupling. This fact implies that the sheath model would have a strong influence on the discharge characteristics of the RF plasma.

5.2. The influence of the sheath thickness

In the circuit model discussed above, the sheath resistance adjacent to the quartz tube is neglected because the sheath voltage drop is assumed to be a floating potential.[7] However, the potential drop can exceed the floating potential as shown in our PIC simulation for micro ICP discarges.[12] After including this sheath resistance R_{sh1} calculated by the same way as R_{sh2} with the difference of the sheath area, we can modify the equivalent circuit model of CCP branch as shown Fig. 12.

5.2.1. Absorbed power and efficiency

Figure 13 shows the power coupling efficiency as a function of RF frequency with and without the sheath resistance adjacent to the quartz tube R_{sh1}. At higher frequency (> 100 MHz), there is almost no difference between including R_{sh1} and not including. However, at lower frequency, the power coupling efficiency significantly increases by including R_{sh1}. Although the current tends to flow through the capacitance rather than the resistance in parallel circuit at higher frequency and the effect of capacitance dominates over that of resistance, the resistance tends to have non-negligible effects at lower frequency. This tendency is clearly seen in the sheath thickness as a function of RF frequency as shown in Fig. 14, where the sheath thickness significantly change by including the sheath resistance R_{sh1} at lower frequency. Similarly, the total resistance R_{cap} and reactance X_{cap} with the sheath resistance R_{sh1} of the CCP circuit branch are almost the same as those without R_{sh1} at higher frequency, while there are large differences between R_{cap} and X_{cap} with R_{sh1} and those without R_{sh1} at lower frequency as shown in Figs. 15 and 16. This drastic impedance change of the CCP circuit branch results in the reduction of the current flowing into the ICP circuit branch and the other transmission line, where the power loss occurs. Therefore, the power coupling efficiency increases at lower frequency by including the sheath resistance R_{sh1}.

Since the efficiency is improved in lower frequency, the power coupling efficiency could be more than 80% when RF frequency is more than 30 MHz and even over 90% when RF frequency is more than 100 MHz. At lower frequency, the effect of the sheath resistance cannot be neglected, so that modified circuit model of CCP branch should be employed. This is due to the fact that the statistical heating in the sheath cannot be ignored owing to the thicker sheath structure. Finally, the maximum power coupling efficiency was obtained at around 100 MHz, which is in agreement with the previous results.[2]

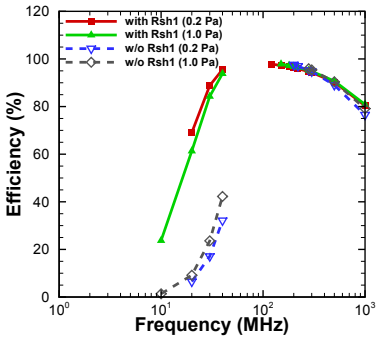

Fig. 13. Power coupling efficiency vs. RF frequency with and without the sheath resistance R_{sh1}.

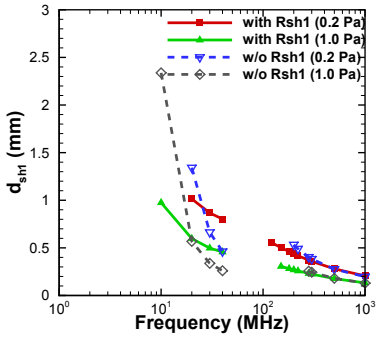

Fig. 14. The sheath thickness near to the dielectric with the improved circuit model.

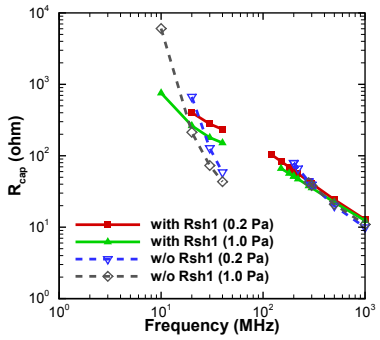

Fig. 15. Total resistance of the CCP circuit branch vs. RF frequency with and without the sheath resistance R_{sh1}.

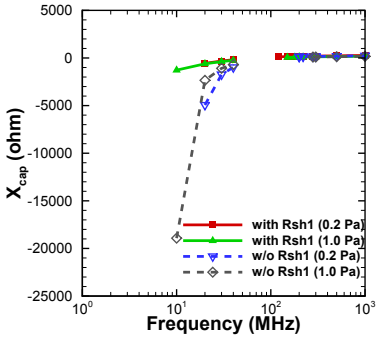

Fig. 16. Total reactance of the CCP circuit branch vs. RF frequency with and without the sheath resistance R_{sh1}.

6. Conclusions

In this study, we have conducted the analysis on micro RF ion thruster by the equivalent circuit model and the global model. The plasma source is 5.0 mm in radius and 10 mm in length with a 5-turn helical coil around a cylindrical quartz tube, where xenon is employed as a propellant gas. The analysis was carried out for the wide range of frequency f = 1-1000 MHz and pressure p = 0.1-10.0 Pa to find the optimum condition to generate the RF plasma. The numerical results have indicated that capacitive coupling dominated over inductive coupling in all the frequency range examined. Since the effect of the sheath resistance cannot be neglected at lower frequencies (< 100 MHz), the power coupling efficiency could be improved by taking into account the sheath resistance in the circuit model. Finally, the maximum power coupling efficiency (> 90%) was obtained at around 100 MHz. As the next step, we will employ the distributed constant circuit model because in this frequency band, the electrical wavelength would have a non-negligible effect.

Acknowledgments

This work was financially supported in part by Casio Science Promotion Foundation, the Sumitomo Foundation, and the Foundation for the Promotion of Ion Engineering. Part of the computer simulation was performed on the KDK computer system at Research Institute for Sustainable Humanosphere, Kyoto University.

References

1) Micci, M. M. and Ketsdever, D. A.: *Micropropulsion for small spacecraft*, American Institute of Aeronautics and Astronautics, Reston, 2000.
2) Takao, Y., Sakamoto, M., Eriguchi, K. and Ono, K.: Investigation of plasma characteristics and ion beam extraction for a micro rf ion thruster, *Trans. JSASS Aerospace Tech. Japan*, **12** (2014), pp. Pb_13-Pb_18.
3) Tsay, M., Hohman, K., Rosenblad, N., Ehrbar, E. and Robin, M.: Micro Radio-Frequency Ion Propulsion System, *Proceedings of the 48th AIAA/ASME/SAE/ASEE Joint Propulsion Conference & Exhibit*, Atlanta, Georgia, (2014), AIAA-2012-3947.
4) Goebel, M. D.: Analytical Discharge Model for RF Ion Thrusters, *IEEE Trans. Plasma Sci.*, **36** (2008), pp. 2111-2121.
5) Charbert, P., Monreal, A. J., Bredin, J., Popelier, L. and Aanesland, A.: Global model of a gridded-ion thruster powered by a radiofrequency inductive coil, *Phys. Plasmas*, **19** (2012), pp. 073512-1-7.
6) Kortshagen, U., Gibson, D. N. and Lawler, E. J.: On the E-H mode transition in RF inductive discharges, *J. Phys. D: Appl. Phys.*, **29** (1996), pp. 1224-1236.
7) Yoshiki, H.: Equivalent circuit model of an inductive rf discharge with a helical external coil, *Jpn. J. Appl. Phys.*, **39** (2000), pp. 598-601.
8) Lieberman, A. M. and Lichtenberg, J. A.: *Principle of Plasma Discharges and Material Processing*, Wiley, Hoboken, 2005.
9) Goebel, M. D. and Katz, I.: *Fundamentals of Electric Propulsion: Ion and Hall Thrusters*, Wiley, Hoboken, 2008.
10) Iza, F. and Hopwood, J.: Influence of operating frequency and coupling coefficient on the efficiency of microfabricated inductively coupled plasma sources, *Plasma Sources Sci. Technol*, **11** (2002), pp. 229-235.
11) Ooi, K. : *Smith chato zissen katuyou gaido (Practical use guide for Smith chart)*, CQ Publishing, Tokyo, 2006 (in Japanese).
12) Takao, Y., Eriguchi, K. and Ono, K.: Effect of capacitive coupling in a miniature inductively coupled plasma source, *J. Appl. Phys.*, **112** (2012), pp. 093306-1-10.